A&A 589, A70 (2016)
DOI: 10.1051/0004-6361/201527875

Astronomy & Astrophysics

The *Gaia*-ESO Survey: membership and initial mass function of the γ Velorum cluster⋆,⋆⋆

L. Prisinzano[1], F. Damiani[1], G. Micela[1], R. D. Jeffries[2], E. Franciosini[3], G. G. Sacco[3], A. Frasca[4], A. Klutsch[4], A. Lanzafame[4,5], E. J. Alfaro[6], K. Biazzo[4], R. Bonito[7], A. Bragaglia[8], M. Caramazza[1], A. Vallenari[9], G. Carraro[10], M. T. Costado[6], E. Flaccomio[1], P. Jofré[11], C. Lardo[12], L. Monaco[13], L. Morbidelli[3], N. Mowlavi[14], E. Pancino[8], S. Randich[3], and S. Zaggia[9]

[1] INAF−Osservatorio Astronomico di Palermo, Piazza del Parlamento 1, 90134 Palermo, Italy
e-mail: loredana@astropa.inaf.it
[2] Astrophysics Group, Keele University, Keele, Staffordshire ST5 5BG, UK
[3] INAF−Osservatorio Astrofisico di Arcetri, Largo E. Fermi 5, 50125 Florence, Italy
[4] INAF−Osservatorio Astrofisico di Catania, via S. Sofia 78, 95123 Catania, Italy
[5] Dipartimento di Fisica e Astronomia, Università di Catania, via S. Sofia 78, 95123 Catania, Italy
[6] Instituto de Astrofísica de Andalucía-CSIC, Apdo. 3004, 18080 Granada, Spain
[7] Dip. di Fisica e Chimica, Università di Palermo, P.zza del Parlamento 1, 90134 Palermo, Italy
[8] INAF−Osservatorio Astronomico di Bologna, via Ranzani 1, 40127, Bologna, Italy
[9] INAF−Padova Observatory, Vicolo dell'Osservatorio 5, 35122 Padova, Italy
[10] European Southern Observatory, Alonso de Cordova 3107 Vitacura, Santiago de Chile, Chile
[11] Institute of Astronomy, University of Cambridge, Madingley Road, Cambridge CB3 0HA, UK
[12] Astrophysics Research Institute, Liverpool John Moores University, 146 Brownlow Hill, Liverpool L3 5RF, UK
[13] Departamento de Ciencias Fisicas, Universidad Andres Bello, Republica 220, Santiago, Chile
[14] Department of Astronomy, University of Geneva, 51 chemin des Maillettes, 1290 Versoix, Switzerland

Received 1 December 2015 / Accepted 21 January 2016

ABSTRACT

Context. Understanding the properties of young open clusters, such as the initial mass function (IMF), star formation history, and dynamic evolution, is crucial for obtaining reliable theoretical predictions of the mechanisms involved in the star formation process.
Aims. We want to obtain a list that is as complete as possible of confirmed members of the young open cluster γ Velorum, with the aim of deriving general cluster properties such as the IMF.
Methods. We used all available spectroscopic membership indicators within the *Gaia*-ESO public archive, together with literature photometry and X-ray data, and for each method, we derived the most complete list of candidate cluster members. Then, we considered photometry, gravity, and radial velocities as necessary conditions for selecting a subsample of candidates whose membership was confirmed by using the lithium and Hα lines and X-rays as youth indicators.
Results. We found 242 confirmed and 4 possible cluster members for which we derived masses using very recent stellar evolutionary models. The cluster IMF in the mass range investigated in this study shows a slope of $\alpha = 2.6 \pm 0.5$ for $0.5 < M/M_{\odot} < 1.3$ and $\alpha = 1.1 \pm 0.4$ for $0.16 < M/M_{\odot} < 0.5$, and it is consistent with a standard IMF.
Conclusions. The similarity of the IMF of the young population around γ^2Vel to that in other star-forming regions and the field suggests it may have formed through very similar processes.

Key words. stars: pre-main sequence – open clusters and associations: individual: γ Velorum – stars: formation – stars: luminosity function, mass function – techniques: radial velocities – techniques: spectroscopic

1. Introduction

The γ Velorum cluster hosts a population of 5−10 Myr old pre-main sequence (PMS) stars, located at 356 ± 11 pc (Jeffries et al. 2009). Owing to its relatively small distance, it appears very dispersed on the sky. It does not show evidence of ongoing star formation and is thus an ideal target for studies of young stars in which the accretion phenomena have already almost ceased entirely (Hernández et al. 2008). The most massive member is γ^2 Velorum, a binary system formed by a Wolf-Rayet (WC8) component of $\sim 9 \pm 2\,M_{\odot}$ and an OIII star of $30 \pm 2\,M_{\odot}$ (De Marco & Schmutz 1999) whose initial masses were ∼35 and 31 $M_{\odot}$, respectively (Eldridge 2009).

Discovered in X-rays by Pozzo et al. (2000), the cluster was established thanks to its relatively high spatial stellar density around γ^2 Velorum, within a region of about one square degree on the sky. A deep photometric survey of this cluster has been obtained by Jeffries et al. (2009), who also used spectroscopic and X-ray data to identify the photometric cluster sequence.

The γ Velorum cluster was the first observed in the *Gaia*-ESO survey (GES; Gilmore et al. 2012), which is a high-resolution spectroscopic survey using the FLAMES instruments

⋆ Based on observations made with the ESO/VLT, at Paranal Observatory under program 188.B-3002 (The *Gaia*-ESO Public Spectroscopic Survey).
⋆⋆ Table 5 is only available at the CDS via anonymous ftp to cdsarc.u-strasbg.fr (130.79.128.5) or via http://cdsarc.u-strasbg.fr/viz-bin/qcat?J/A+A/589/A70

(both GIRAFFE and UVES) of the ESO-VLT (Pasquini et al. 2002). It aims to obtain a homogeneous overview of the kinematic and chemical abundance distributions of several components of our Galaxy, including a census of ~100 open clusters (OCs). In particular, the GES observation strategy for the OCs is to observe with GIRAFFE all candidate members falling spatially in the cluster area and within the cluster locus of the color-magnitude diagrams (CMD), down to $V = 19$ mag. The aim of this strategy is to observe an unbiased and inclusive sample of candidate cluster members. This observation strategy is adopted to achieve the GES main goals that are to kinematically characterize the entire populations, and, at the same time, homogeneously derive their chemical abundances. For example, a slightly subsolar metallicity was found by Spina et al. (2014) for the γ Velorum cluster. GES data allow also further investigations to be performed, for example to derive fundamental stellar astrophysical parameters and then cluster fundamental parameters, such as reddening, age, distance, and mass. The last are crucial for constraining cluster formation theory (star burst events, sequential star formation, and age spread), stellar evolution models and deriving the initial mass function (IMF).

The first goal of this paper is to establish the membership of the γ Velorum cluster. Starting from an inclusive sample of candidate cluster members, membership will be confirmed or rejected by using radial velocities (RV) and stellar properties (e.g., surface gravity, effective temperature, Li abundance, accretion rates, chromospheric activity, rotation) that can be derived from spectral features falling in the $\lambda\lambda$6440–6815 Å spectral range, which is covered by the GIRAFFE HR15N set-up. The sample of confirmed members is used to derive the IMF.

In a study dedicated to the dynamical analysis of this cluster, using the very precise RVs derived with GES, Jeffries et al. (2014) found that the cluster consists of two distinct kinematic populations, referred to as A and B, with ages of about 10 Myr, of which population B is, on the basis of Li depletion, judged to be 1–2 Myr older than population A. Since the cluster is located in the region of the Vela OB2 association (de Zeeuw 1999), the authors conclude that population A is the remnant of an initially much denser cluster, formed in a denser region of the Vela OB2 association, while population B is more extended and supervirial.

This scenario is coherent with that found by Sacco et al. (2015), who studied the RV distribution from GES data of the cluster NGC 2547 in the same direction as Vela OB2 and found an additional population, kinematically distinct from NGC 2547, but consistent with population B of γ Vel (see also Mapelli et al. 2015).

In the case of the γ Velorum cluster, it is very likely that populations A and B belong to the same parent nebula, and even if the two populations are kinematically distinct, they are almost indistinguishable in the CMD, and this implies they have very similar distance and ages. In addition, they share very similar spectroscopic properties, as already shown in Jeffries et al. (2014). For the aims of this work, we thus consider the two populations A and B as a single young population.

2. Targets and astrophysical parameters

The GES targets observed in the γ Velorum cluster region were selected as described in Jeffries et al. (2014), following the GES observational strategy (Bragaglia et al., in prep.). Candidate cluster members were observed with FLAMES at the VLT using both the GIRAFFE intermediate-resolution and the UVES high-resolution spectrographs. Details of the GES observations of the γ Velorum cluster are reported in Jeffries et al. (2014). For our analysis we only use GIRAFFE data, while we do not consider UVES data since the sample of stars observed with UVES is not complete, as required for our analysis. GIRAFFE spectra analyzed in this work were reduced using the pipeline developed at the Cambridge Astronomical Survey Unit (CASU) in collaboration with Keele University, as described in Lewis et al. (in prep.).

There were 1242 targets observed with GIRAFFE in the field of γ Vel, selected on the basis of their positions in the optical CMDs, but covering a very wide range around the CMD cluster locus. Since some targets were observed more than once, the data set includes 1802 spectra.

The stellar parameters used in this work were taken from the last data release (gesiDR2iDR3) of the GES official archive at the Wide Field Astronomy Unit (WFAU) of Edinburgh University[1]. In particular we used the RVs from the RecommendedAstroAnalysis table for the 1122 targets for which the RVs are given and the RVs from the spectrum table for the 99 targets for which the RVs are not given in the RecommendedAstroAnalysis table. The RVs from the spectrum table were shifted by -0.13 km s^{-1} to have the RVs in the same reference system. In total we have a RV value for 1221 objects of the entire sample. The errors on the RV were computed by using the RV precision recipe given in Jackson et al. (2015). In addition, we used the projected rotational velocities $v \sin i$ from the spectrum table, while the equivalent width of the lithium line EW(Li), the full width at 10% of the Hα peak (Hα 10%), the chromospheric equivalent width of the Hα line, and the gravity index γ (defined in Damiani et al. 2014) were taken from the WgRecommendedAstroAnalysis table (Lanzafame et al. 2015). We also used the α_c index of chromospheric activity based on GES data from Damiani et al. (2014). Finally, we used the optical literature photometry and the EPIC-*XMM-Newton* X-ray data from Jeffries et al. (2009).

Double-lined spectroscopic binaries (SB2) were identified by examining the shape of the cross-correlation function, while SB1 were classified on the base of their RV in case of multiple observations (Lanzafame et al. 2015). In particular, the WgRecommendedAstroAnalysis table of the γ Velorum field includes 23 SB1 and 21 SB2 stars, respectively.

3. Membership criteria

We describe here all the adopted criteria used to select candidate members of the young cluster γ Velorum. The conditions that we applied select the maximum number of possible members for each method. This implies including a significant fraction of contaminants, but, as we describe in Sect. 4, the final membership is based on the necessary conditions from photometry, gravity, RV, and an age criterion. The age criterion is based on either Li abundance, stellar activity, or X-ray emission, one of those criteria being sufficient. This strategy ensures the selection of the maximum number of cluster members.

3.1. Photometric membership

As described above, the survey strategy is to select targets in a photometric region of the CMD larger than that expected for the cluster age. Then in the following analysis we consider as high-probability photometric cluster members the 579 objects that in the V vs. $V - I$ diagram fall between the 0.5 and 20 Myr theoretical isochrones from Baraffe et al. (2015), reddened by

[1] http://ges.roe.ac.uk/index.html

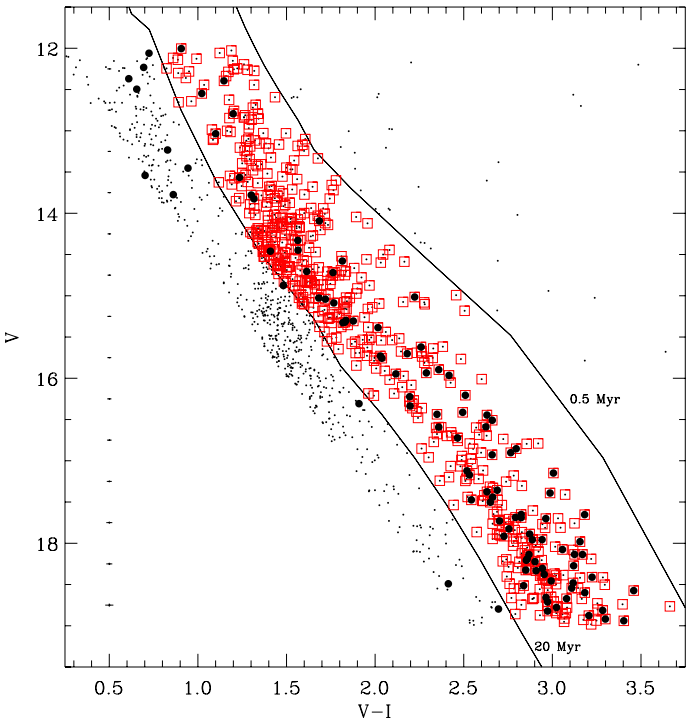

Fig. 1. Color magnitude diagram of all the 1242 targets observed in the γ Velorum field (dots). Empty red squares are the 579 photometric candidate members and black filled circles are X-ray detected objects. Solid lines are 0.5 and 20 Myr isochrones from Baraffe et al. (2015). Typical photometric error bars are also indicated.

$E(V-I) = 0.055$ and $A_V = 0.131$, at an intrinsic distance modulus of 7.76 (Jeffries et al. 2009), as shown in Fig. 1. To fix these age limits, we were guided by the position of the X-ray-detected objects in the CMD, since most of them are expected to be cluster members (see Sect. 3.6) and thus trace the cluster sequence. With these limits we are confident of including all possible cluster members, but we are aware of including a large number of contaminants. However, since we consider other membership criteria, most of the contaminants are discarded in the final selection.

Very young stars with a circumstellar disk and/or accretion can also be photometrically selected by considering the IR $J-H$ vs. $H-K$ diagram where they lie in the well known classical T Tauri star (CTTS) locus, which is a region with IR excesses well outside from the locus of the main sequence (MS) or giant stars. This is a way of including additional members, identified by the presence of discs/accretion. We verified that in this cluster, only three of the selected GES targets fall in the CTTS locus[2], and so we do not consider the IR color-color diagram as a useful method of selecting young stars in this cluster.

3.2. Radial velocities

The radial velocity membership criterion is based on the assumption that in a given cluster, members share similar RVs and have a narrow RV distribution. Since our sample of targets has been selected photometrically, we expect to find a fraction of contaminant field stars that have a much broader RV distribution, overlapping that of the cluster. Our aim is then to model the cluster and field RV distributions to derive the RV range of cluster members.

A scrupulous analysis to model the RV cluster distribution has been presented in Jeffries et al. (2014), who considered an unbiased sample of 208 γ Velorum members and computed, for each member, the likelihood of having the observed RV. This likelihood has been computed by convolving an intrinsic RV distribution with the measurement uncertainties and the distribution of velocities expected for a given percentage of binaries. By using a maximum likelihood fit, it has been shown that the cluster RV distribution is represented better if the intrinsic RV distribution is modeled with a two-Gaussian fit, highlighting the presence of the two kinematic populations A and B in the direction of the γ Velorum cluster.

We used the cluster probability density function (PDF) computed by Jeffries et al. (2014)[3] to derive the RV range where we can find cluster members. In particular, by computing the PDF area within a given RV range, we fixed the RV limits for the cluster to the values for which the probability of finding cluster members is lower than 0.003 (equivalent to 3σ level) for objects with RV outside this range. These limits correspond to $[RV_{inf}, RV_{sup}] = [1.8, 36.5]\,km\,s^{-1}$. The number of cluster members with RVs within this range is 541, while that with RVs outside this range is expected to be 0.3, so this is the best compromise to not miss cluster members even though this implies including of a significant number of contaminants. We are not considering here the possibility or probability that there is a population of binary systems with a broader RV distribution, and so some member binaries may be missed on the basis of their RV.

In addition, for several aims of this work, we also defined a more conservative cluster RV range corresponding to a 2σ confidence level. With these conservative RV limits $[RV'_{inf}, RV'_{sup}] = [12.3, 23.5]\,km\,s^{-1}$, we selected a less complete (we expect to miss about 5 cluster members with RV outside these limits) but less contaminated sample of cluster members that, combined with other conditions, allow us to select a fiducial sample of almost certain cluster members.

To compute the contaminant fraction, we fit the field RV distribution by using the entire RV data set without the objects with RVs within the more conservative cluster RV range $[RV'_{inf}, RV'_{sup}]$. We modeled this field RV distribution with a Gaussian function by using maximum likelihood fitting and found that the RV mean of the field RV distribution is $54.7 \pm 1.3\,km\,s^{-1}$ with a $\sigma = 40.2 \pm 0.9\,km\,s^{-1}$.

Figure 2 shows the RV density distribution of the entire data set compared to the total PDF obtained by adding the numeric Jeffries et al. (2014) cluster model to the field PDF derived by us. The two distributions were normalized to the number of objects used to derive the two distributions.

By using this model, we computed the probability to find field stars within the cluster $[RV_{inf}, RV_{sup}]$ range and then the number of contaminants expected in the cluster region that amounts to 268 objects. We note that the adopted field model does not accurately describe our data at $\sim 0\,km\,s^{-1}$ and $\sim 30\,km\,s^{-1}$, where there is an excess of stars in the observed distribution. This excess could be due to some additional structures in the RV distribution that we do not include in our fit. For example, large uncertainties in the RV measurements of fast rotators can introduce additional structures in the observed distribution. This suggests to us that the number of contaminants could be larger, so we consider our estimate a lower limit to the

[2] These objects are selected as cluster members with the other methods adopted in this work.

[3] We applied a shift of $-0.13\,km\,s^{-1}$ to the RVs of the model to move the values to the reference system of the RVs of our data.

true contamination. Based on the excess of our data with respect to the model, we estimate that the percentage of missed contaminants amounts to about 10%.

In conclusion, we consider the 541 stars with RV between 1.8 and 36.5 km s^{-1} as candidate members for RV. In this sample we also include the binaries since the RV of the center of mass is supposed to share the cluster RV distribution. Nevertheless, since the method used to derive official GES released RVs does not ensure that the RV of the binaries is that of the center of mass, we are aware that some binary members may be missed on the basis of their RV. The same is true for fast rotators for which the RV uncertainties are typically very large. For this reason, binaries and fast rotators are considered as a special sample in the final cluster member selection in the sense that for them RV membership is not considered a necessary condition, as is instead required for single stars.

3.3. Lithium line

In this section, we assign cluster membership on the basis of the strength of the Li I 6708 Å line, that is a well-known age indicator for young stars, such as those expected to be found in the γ Velorum cluster. As discussed in Jeffries et al. (2014), theoretical isochrones are very uncertain in predicting the lithium depletion pattern, and for this reason we have adopted an empirical approach aimed at highlighting the cluster locus in the EW(Li) vs. $V-I$ diagram to fix the most appropriate EW(Li) thresholds for the cluster member selection. With this aim we used an initial sample of candidate cluster members based on criteria that are free of any bias due to the lithium line. In particular, we defined a cluster member fiducial sample (CMFS) that includes the 235 objects that are both photometric cluster members (as defined in Sect. 3.1) and that have RV within the conservative cluster range ($[RV'_{inf}, RV'_{sup}]$) defined in the previous section. We note that this sample includes not only genuine cluster members since within the photometric cluster locus a fraction of contaminants with RV within the $[RV'_{inf}, RV'_{sup}]$ range is expected. Nevertheless, the sample is strongly dominated by cluster members and can be used to trace their lithium properties. This sample will also be used as reference for the cluster for other membership criteria described in the following sections.

Figure 3 shows EW(Li) vs. $V-I$ color where the CMFS, selected using only the RVs and the position on the CMD, is highlighted in red. Since this cluster is not affected by strong reddening, the $V-I$ colors, at least for cluster members, can be considered as a good proxy for the spectral type (Jeffries et al. 2009; Damiani et al. 2014). We note that, in general, most of the candidate cluster members have EW(Li) larger than 200 mÅ, with a trend depending on the spectral type, as expected from the young ages of these objects. Nevertheless, candidate cluster members with colors in the range $2.5 \lesssim V-I \lesssim 3$, corresponding to stars of spectral type M3 and M4, could have a much weaker line and appear to have begun to deplete their Li.

We use the CMFS to empirically define the cluster locus in this diagram and to distinguish the cluster population from the field stars. Since the EW(Li) of cluster members shows a pattern that depends on color, we define four $V-I$ ranges ([1.0−1.5],[1.5−2.0], [2.0−2.5] and [3.0−3.5]) where the EW(Li) distribution of candidate cluster members is separated well from that of the field stars. This is not the case for the bin $2.5 < V-I < 3.0$, which is treated separately since in this color range, the EW(Li) of cluster members cannot easily be distinguished from those of field stars. For each of these color ranges, we assume that the EW(Li) of the candidate cluster members are drawn from an intrinsic Gaussian distribution that is broadened by uncertainties on the EW(Li). For each color range, the CMFS includes few contaminants with weak lithium that probably belong to the field population, so actually we are dealing with two populations. Therefore we modeled the EW(Li) distribution of the CMFS with two Gaussian components, one

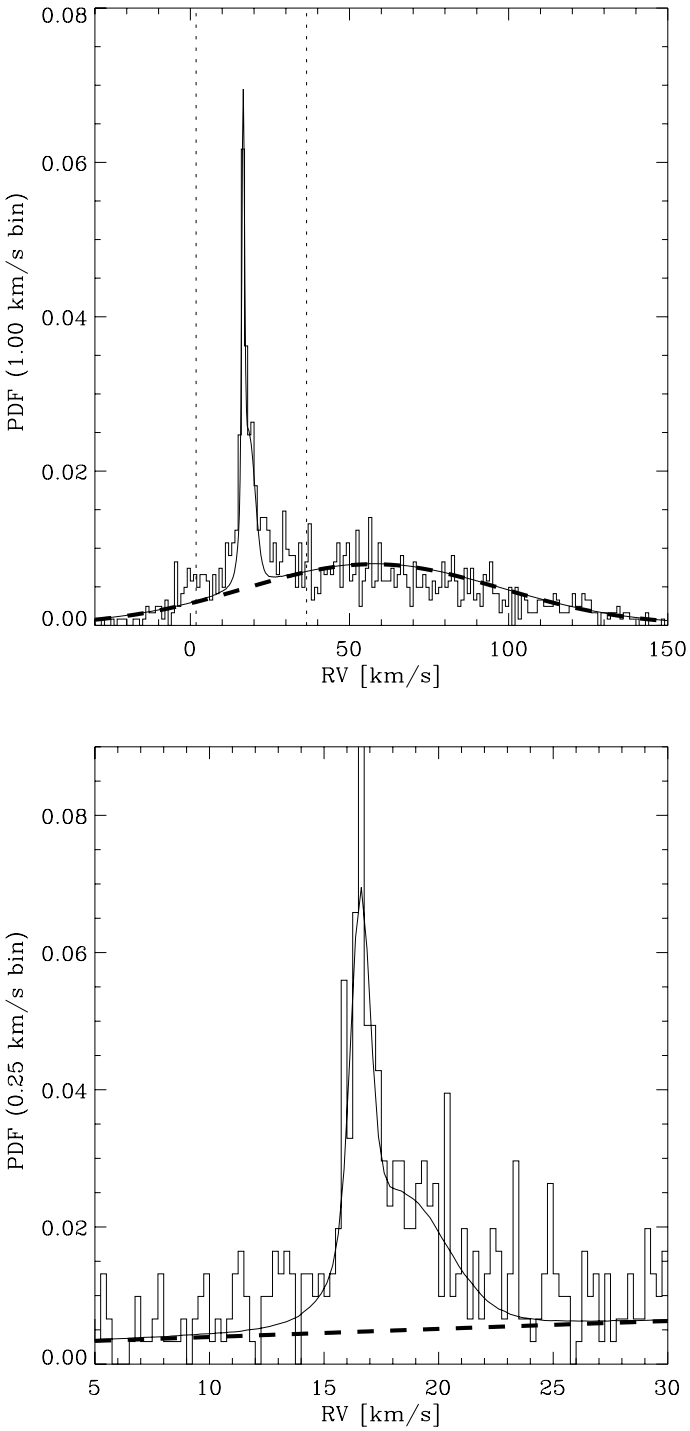

Fig. 2. RV histogram for the entire data set of γ Velorum cluster showing the entire RV range (*upper panel*) and a zoom of the cluster range (*bottom panel*) compared with the total PDF (solid line) obtained by adding the Jeffries et al. (2014) cluster model to the field PDF performed by us (thick dashed line). Vertical dotted lines delimits the $[RV_{inf}, RV_{sup}]$ range used to select RV cluster member candidates.

Table 1. Parameters derived with the maximum likelihood fitting for the EW(Li) PDFs.

$V-I$	$\langle EW(\mathrm{Li})^{\mathrm{Cl}}\rangle$ [mÅ]	$\sigma_{EW(\mathrm{Li})^{\mathrm{Cl}}}$ [mÅ]	$\langle EW(\mathrm{Li})^{\mathrm{F}}\rangle$ [mÅ]	$\sigma_{EW(\mathrm{Li})^{\mathrm{Cl}}}$ [mÅ]	$\frac{N_{\mathrm{F}}}{N_{\mathrm{Tot}}}$	$EW(\mathrm{Li})_{\mathrm{min}}$ [mÅ]
$1.0 < V-I < 1.5$	422.0	38.1	27.9	18.2	0.9	100.7
$1.5 < V-I < 2.0$	487.7	45.1	32.0	19.7	0.9	110.9
$2.0 < V-I < 2.5$	451.4	58.8	45.0	31.7	0.7	171.7
$3.0 < V-I < 3.5$	555.8	68.1	53.3	27.3	0.2	162.3

Notes. Column 1: color range, Cols. 2 and 3: mean and sigma of the cluster PDF, Cols. 4 and 5: mean and sigma of the field PDF, Col. 6: fraction of field stars with respect to the total sample, Col. 7: adopted EW(Li) threeshold.

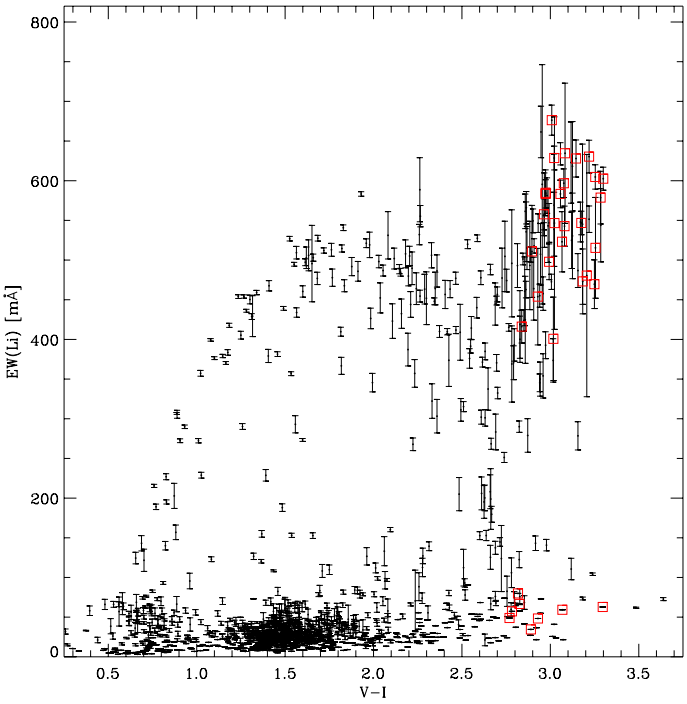

Fig. 3. EW(Li) as a function of the color $V-I$ for all targets observed in the γ Velorum region. Red empty squares are the objects in the CMFS selected from their RV and the position on the CMD.

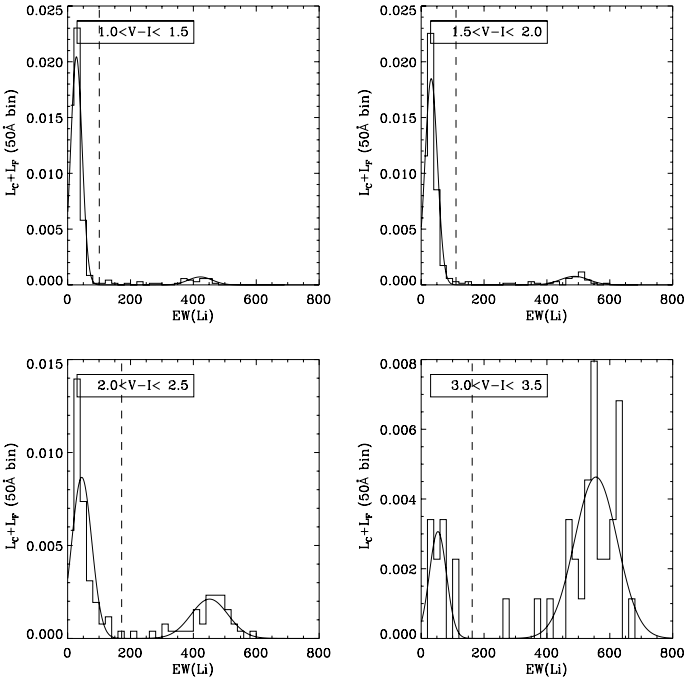

Fig. 4. Comparison between the EW(Li) distributions of all observed targets falling in the selected $V-I$ ranges and the best fit models derived as described in the text. The dashed vertical line in each panel indicates the threshold that has been used to select cluster members.

for the cluster (L_{C}) and one for the field (L_{F}) to take account of the small fraction of contaminants, and fitted the distribution for each color range using a maximum likelihood technique. In this step, we are only interested in the parameters of the cluster (L_{C}), which are given in Cols. 2 and 3 of Table 1.

Next, we considered all the targets of the entire dataset for which an EW(Li) value has been released and that fall in these color ranges. With the maximum likelihood technique, we again fit the sum of the two PDFs, but in this step, we fixed the Gaussian parameters of the cluster L_{C} to the values derived in the first step. The centers and the widths of the EW(Li) distribution of field stars for each color range and the decimal fraction of objects that belong to the field population, as derived in this second step, are given in Cols. 4–6 of Table 1.

Figure 4 shows, for each color range, the comparison of the observed EW(Li) distributions from the entire dataset, with the best fit models derived as described previously. We used these models to derive the best threshold of the EW(Li) to select the maximum number of cluster members whilst minimising the number of contaminants. For each color range, we defined cluster members as those with $EW(\mathrm{Li}) > 4\sigma$ from the mean $EW(\mathrm{Li})$ of the field PDF L_{F} ($EW(\mathrm{Li})_{\mathrm{min}}$). By using the field PDF L_{F}, we computed the probability of finding contaminants with EW(Li) larger than these thresholds (given in Col. 7 of Table 1) and then the number of contaminants that is <0.01. Accordingly, with these thresholds, all possible cluster members are expected to be included.

A different approach has been adopted to derive the membership from the lithium line in the color range $V-I = [2.5–3.0]$. Figure 3 clearly shows that the fraction of Li-poor fiducial cluster members ($EW(\mathrm{Li}) \lesssim 100$ mÅ) with respect to the number of all observed Li-poor targets (21/50 = 0.42) in this color range is relatively high. It is significantly higher than the same fractions in the other color ranges, where we find 13/325 = 0.04, 3/313 = 0.01, and 4/83 = 0.05, in the $V-I$ ranges [1.0–1.5], [1.5–2.0], and [2.0–2.5], respectively. This suggests that a high percentage of the candidate cluster members with very weak lithium and $2.5 < V-I < 3.0$ are actually cluster members. Only a low percentage of the candidate cluster members belong to the field star population, according to their RV.

To estimate the number of expected cluster members among the 21 Li-poor candidates selected for their RV, we need to estimate the number of expected contaminants. We hypothesize that outside the range $2.5 < V-I < 3$, all the Li-poor stars are

unassociated with the cluster. We assume further that these objects have a similar RV distribution to any contaminating field star with $2.5 < V - I < 3$. We find that the number of Li-poor stars (considered as contaminants) with $1.0 < V - I < 2.5$ selected within the CMFS is 20 (13+3+4), and the number of all observed Li-poor targets in the same color range is 721 (325+313+83). Then the number of Li-poor targets not included in the CMFS is 721−20 = 701. Thus the ratio between the contaminants in the CMFS and those outside the CMFS is 20/701 = 0.028. If we assume the same ratio in the $2.5 < V - I < 3$ range, then the number of expected contaminants in the CMFS is 0.028*(50−21) = 0.83 ≃ 1. Therefore, the number of expected Li-poor cluster members is 21−1 = 20. For this reason, we cannot rule out that Li-poor targets in this color range are cluster members. Since we cannot individually assign their membership based on the Li line, we consider them as undefined according to Li, leaving them the chance to be selected as cluster members with other membership criteria.

Finally, for $V - I < 1$, where most of G-type stars are expected to be found, the strength of the lithium line is no longer a sensitive age indicator since these stars do deplete lithium on the zero age main sequence (Sestito et al. 2003). For this reason, in this color range, we consider the 14 objects with $EW(\mathrm{Li}) > 100$ mÅ, as undefined according to the Li, while the remaining 154 are considered non members. We do not consider the four stars with $3.5 < V - I < 5$ and $EW(\mathrm{Li}) < 200$ mÅ as cluster members, since in this color range they are expected to have $EW(\mathrm{Li}) > 200$ mÅ.

After this selection we have 225 objects with EW(Li) larger than the threshold chosen in each color range, and they are considered cluster members according to the Li test, 897 non-members and 120 objects that are undefined according to Li. The last sample includes the 56 objects for which the EW(Li) has not been measured, the 50 objects with $EW(\mathrm{Li}) < 100$ mÅ and $2.5 < V - I < 3.0$, and the 14 stars with $V - I < 1$ and $EW(\mathrm{Li}) > 100$ mÅ. Figure 5 shows the EW(Li) distribution as a function of the $V - I$ colors, where the sample of candidate cluster members selected with the Li line is highlighted.

For binary stars it is sufficient that one of the two components has an EW(Li) larger than the adopted threshold to consider it as a young star. However, in the case of candidate binaries, both SB1 and SB2, it is not possible to disentangle the continuum of the two components. In addition, not even the two lines can be disentangled in the case of unresolved SB2 binaries. This implies that the measured EW(Li) can be overestimated or underestimated. Nevertheless, we considered the binary stars as single stars, with the risk of missing cluster members and/or including some contaminants, This is consistent with our choice of being inclusive in the selection of candidate members with each criterion taken separately.

3.4. Hα line

Spectra of young stars can show the Hα line in emission for several physical reasons, such as chromospheric activity or accretion of circumstellar material toward the star. This last process can also be associated with outflows from the central star. However, while chromospheric activity affects the core of the line by filling it and possibly emerging as a narrow Hα emission line, accretion and outflow processes affect the line wings, causing a significant broadening. The Hα line broadening arises from the gas motion that implies a strong enhancement of the gas temperature due to the shock produced when the circumstellar

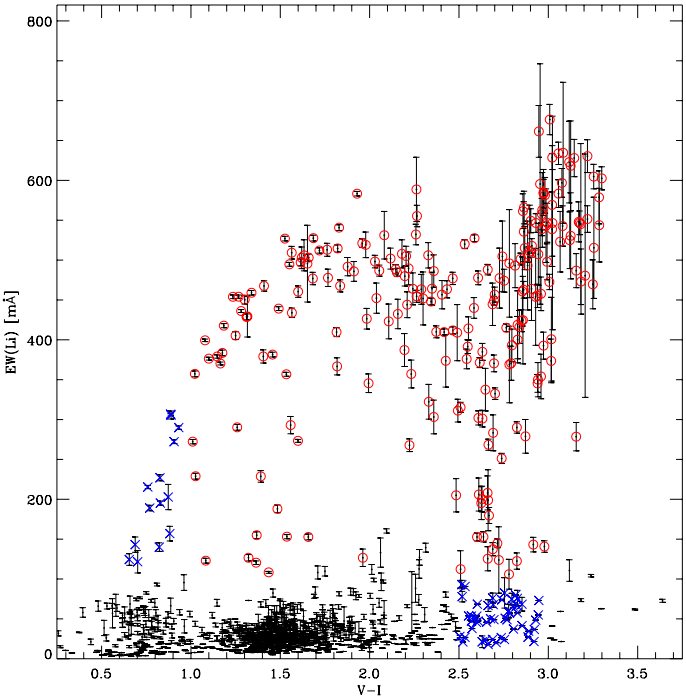

Fig. 5. EW(Li) as a function of the color $V - I$ for all targets observed in the γ Velorum region. Red empty circles are candidate cluster members selected for the Li line criterion, whereas blue crosses are the 64 objects which are left undefined according to the Li test.

material, driven by the magnetic field lines, impacts the stellar surface. In some case, a depression is also observed in the redward wing that is a signature of an infalling envelope (Bertout et al. 1996).

A detailed study of the properties of the Hα emission profiles for the spectra observed within the *Gaia*-ESO survey has been presented in Traven et al. (2015). Their analysis highlights several morphologic types of the Hα emission, including the intrinsic emission and the nebular contribution.

With an age of 5−10 Myr (Jeffries et al. 2009), the γ Velorum cluster could host young stars with accretion, outflows, or chromospheric activity. The Hα emission properties from GES spectra for a sample of selected members of the γ Velorum cluster have been extensively studied by Frasca et al. (2015), who classified accretor stars by using the full width at 10% of the Hα peak (Hα 10%). In addition, they studied chromospheric activity by using the net Hα equivalent width derived with a spectral subtraction method (Frasca & Catalano 1994). This measurement is based on the removal of the photospheric flux to obtain the chromospheric emission of the line core. Their analysis is restricted to the sample of 137 γ Velorum members selected as in Jeffries et al. (2014) with GES spectra having a signal-to-noise ratio $(S/N) > 20$.

Based on the previously mentioned properties, the Hα line shape can be used as a membership criterion since it allows us to distinguish accretors and young active stars from non-active older stars.

In the following sections we start from the entire GES data set in the γ Velorum field, to describe how we selected spectra with very broadened Hα line, typical of accretors, and spectra with narrow Hα emission line, which is characteristics of chromospheric activity.

3.4.1. Accretor selection

Young stars with accretion are usually selected as objects with a Hα 10% width >270 km s^{-1} (Muzerolle et al. 2000; White & Basri 2003; Frasca et al. 2015). By applying this condition to the entire set of GES data in the γ Velorum cluster, we select 26 objects. However, since most of the targets observed in the γ Velorum field are M-type stars and a large percentage of them are also fast rotators, we checked if the broadening observed in the Hα line occurs also in the other spectral lines, rather than only in the Hα line, as expected in the case of accretion.

To this aim, we estimated the line spectral broadening due to rotation from the FWHM of a rotational (not limb-darkened) line profile, i.e.,

$$\Delta\lambda_{\rm Rot} = 2 \times \frac{\sqrt{3}}{2} \frac{v \sin i \lambda_0}{c} \quad (1)$$

where λ_0 is the rest wavelength and $v \sin i$ is the projected rotational velocity. Figure 6 shows the $\Delta\lambda_{\rm Rot}$ as a function of the Hα 10%. It is evident that for a subsample of stars with high Hα 10% (>200 km s^{-1}), $\Delta\lambda_{\rm Rot}$ is correlated to the Hα 10% and so for these objects the observed broadening of the Hα line is likely due to the fast rotation rather than to accretion. These objects were not considered accretors. On the contrary, the stars with high Hα 10% but low $\Delta\lambda_{\rm Rot}$ are considered here to be certain accretors.

In conclusion, we selected as accretors those with Hα 10% larger than 270 km s^{-1} and $\Delta\lambda_{\rm Rot}$ smaller than the limit (arbitrary chosen) traced by the dashed line ($\Delta\lambda_{\rm Rot} < 0.22 \times$ Hα10%$-$10). With these conditions, we selected eight young stars.

We compared our results with those obtained by Frasca et al. (2015) and found that four of the eight stars classified here as accretors were also classified by Frasca et al. (2015). The remaining four accretors were not classified by Frasca et al. (2015) since three of them were not included in their sample, and in another case, the iDR1 Hα 10%$-$10 value used by Frasca et al. (2015) was 196.5, i.e., lower than the limit adopted to select accretors.

Finally, there are four accretors (CNAME = 08083838-4728187, 08094046-4728324, 08104993-4707477, and 08085661-4730350) classified by Frasca et al. (2015) that were discarded by us, since their Hα 10% values are strongly correlated with the expected rotational broadening, and we suspect that for these objects, the Hα line broadening is more related to fast rotation rather than accretion.

Since spectra can be variable, especially in case of accretion, for stars observed more than once, we visually inspected the Hα line morphology using the single acquired spectra for each target. We found that both spectra of the star J08075546-4707460 show a P-Cygni profile, with variable intensity in both emission and absorption components. In addition, the two components are correlated in the sense that when the emission intensity decreases, also the absorption decreases. In conclusion, we have eight stars classified as accretors, including one star with a P Cygni Hα profile. These targets are listed in Table 2, where the objects classified by Frasca et al. (2015) are also indicated.

3.4.2. Active star selection

Even without accretion activity, young stars with outer convection zones would usually be expected to show narrow Hα as a result of magnetically induced chromospheric activity that is ultimately due to their relatively fast rotation. Angular momentum loss and spin-down then lead to the fading of chromospheric activity with age, but on a mass-dependent timescale – while solar-type stars cease to display Hα emission on timescale of ~100 Myr, there can be Hα emission in lower mass M dwarfs even at ages of 1 Gyr and beyond (Bochanski et al. 2007). Thus narrow Hα emission lines can be used as a mass-dependent indicator of a youthful status and thus as a condition for assigning cluster membership in combination with other criteria.

As in Frasca et al. (2015), to define active stars we considered the net Hα equivalent width (EWHaChr) values from the GES recommended parameters, available for 205 of the entire sample of observed stars. In addition, we used the α_c index derived by Damiani et al. (2014) that measures the Hα core (2 Å from the line center) in cases of both emission and absorption. It has been measured for 1153 stars of our sample.

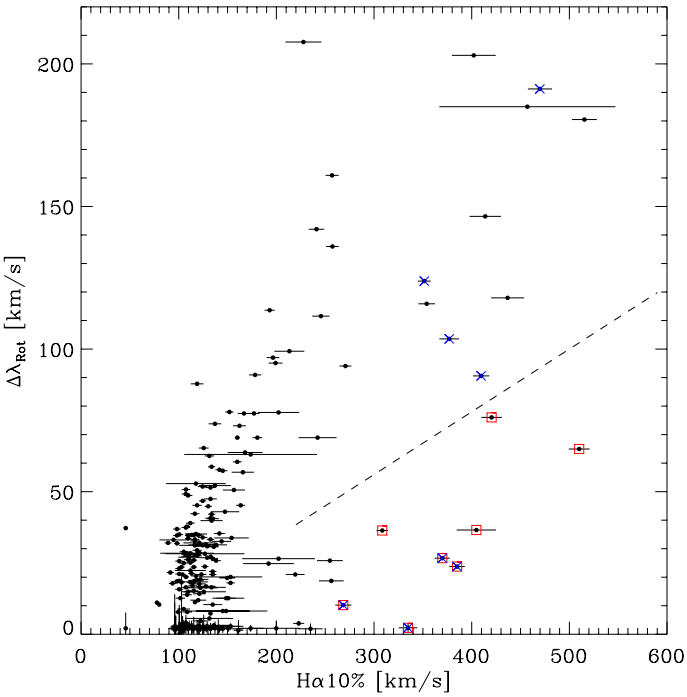

Fig. 6. FWHM of the line spectral broadening due to rotation as a function of the Hα 10%. Empty squares indicate objects classified here as accretors, while crosses indicate the accretors selected by Frasca et al. (2015).

Table 2. Revised candidate accretor list in γ Velorum.

Star	FW10% km s^{-1}	Accr. flag This work	Result FBL15
08065672-4712133	404.8 ± 20.2	Yes	No
08075546-4707460	308.4 ± 5.9	Yes-PCyg	No
08082236-4710596	510.1 ± 10.7	Yes	No
08083838-4728187	377.0 ± 10.1	No	Yes
08085661-4730350	420.4 ± 10.6	Yes	No
08094046-4728324	469.9 ± 12.3	No	Yes
08100280-4736372	369.9 ± 7.7	Yes	Yes
08103074-4726219	268.5 ± 8.2	Yes	Yes
08104649-4742216	334.8 ± 9.5	Yes	Yes
08104993-4707477	351.4 ± 6.6	No	Yes
08105600-4740069	385.0 ± 7.9	Yes	Yes
08110328-4716357	409.7 ± 8.3	No	Yes

Notes. Column 1 is the CNAME; Col. 2 is the FW at 10% of the Hα peak, Col. 3 is the result obtained in this work, Col. 4 is the result obtained by Frasca et al. 2015 (FBL15).

Figure 7 shows the chromospheric EW(Hα) as a function of the α_c index (upper panel) and the α_c index as a function of the $V-I$ color (lower panel). It is evident that, for Log $(EW(H\alpha_{Chr})) > -0.5$, the chromospheric EW(H$\alpha$) is well correlated to the α_c index (upper panel). In addition, most of the cluster members show a characteristic trend to high α_c values as a function of $V-I$ (lower panel) that describes the chromospheric emission dependence on spectral type (Damiani et al. 2014). Objects with Hα absorption line have low α_c values according to the α_c index definition.

Since the α_c values are given for almost the entire sample of GES observed targets, we used this index to select stars with chromospheric activity. In particular, by following the trend of the α_c index of the RV candidate cluster members, we define the 242 objects with $V-I > 0.8$ and Log $\alpha_c > 0.13(V-I) - 0.25$ (dashed line) selected from spectra with $S/N > 15$ as active stars.

The selected stars correspond to objects with Log $EW(H\alpha_{Chr}) > -0.5$ that can also be considered as a threshold to select confirmed active stars. We discard objects with Log $EW(H\alpha_{Chr}) < -0.5$ since they show very small chromospheric activity and the EW(Hα_{Chr}) is affected by large errors.

To the sample of selected active members, we added the four objects with Log $(EW(H\alpha_{Chr})) > -0.5$ that were not selected in the previous step since their α_c index is slightly smaller than the threshold we adopted. In total we selected 246 candidate cluster members on the basis of their chromospheric activity, ten of which were already selected as accretors.

3.5. Candidate members from gravity

The γ index, which is defined using strongly gravity-sensitive lines (Damiani et al. 2014), is an efficient gravity indicator and allows a clear separation between the low gravity giants and the higher gravity MS and PMS stars, starting from early G-type stars. Even if with a lower confidence level, this index also allows us to distinguish MS from PMS stars. Figure 8 shows the γ index as a function of the $V-I$ color for the 1043 objects for which the index has been released with the GESiDR2iDR3. Objects with $\gamma \gtrsim 1$ are giant stars, while those in the bottom region of the plot are MS and PMS stars. By using the CMFS, we see that most of the stars of the CMFS, which are expected to be PMS stars, have γ index values in the upper envelope of the region of high gravity objects ($\gamma \lesssim 1$), while MS stars lie in the lower part of the same envelope. We note that this sample does not include the fast rotator stars ($v \sin i > 30\,\mathrm{km\,s^{-1}}$) for which the γ index value can be altered by the large line widths (Damiani et al. 2014).

Based on the γ index, we consider the candidate giants, i.e., all the 592 objects with $\gamma > 1.0$ and $V-I > 1.2$, delimited by the dashed lines in the figure, as high-probability cluster non-members. These objects correspond to stars with $\log g \lesssim 3.2$ and $T_{\rm eff} \lesssim 5600$ K. By using the Siess et al. (2000) models, we find that PMS stars with $T < 5200$ K, older than 1 Myr, have $\log g$ always greater than ~3.2, and therefore we are confident that the objects we are discarding are not PMS stars. We consider all the remaining 648 objects as potential candidate cluster members.

We are aware that by adopting the *arbitrary* limit $\gamma = 1.0$, we are including a small percentage of candidate giants with $\gamma \lesssim 1.0$ in our sample of candidate cluster members. This choice agrees with our strategy of including all possible candidate cluster members.

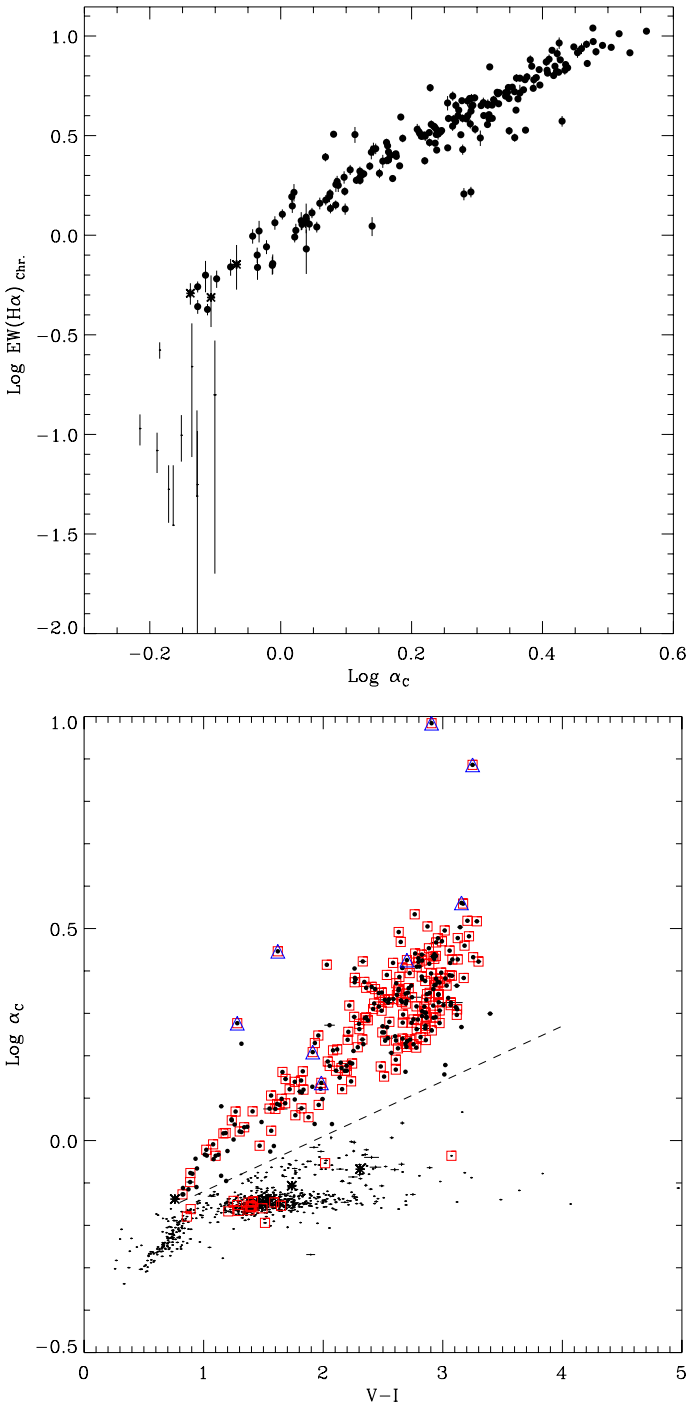

Fig. 7. *Upper panel*: EW(Hα)$_{Chr}$ as a function of the α_c index. *Lower panel*: Log α_c index as a function of the $V-I$ color (dots). Empty squares are the objects from the CMFS and triangles indicate the objects selected as accretors. Filled circles are the active candidate members selected on the basis of the α_c index, while asterix symbols are those selected on the basis of the EW(Hα)$_{Chr}$. The dashed line indicates the lower limit used for the selection with the α_c index.

This last sample includes the 451 stars that are MS or PMS stars and the 199 objects for which the gravity index is undefined and for which membership can be assigned by using the other methods. We note that with a low confidence level, MS could be distinguished by PMS stars but we adopt the inclusive approach to include even objects that are MS stars in our sample of candidate cluster members.

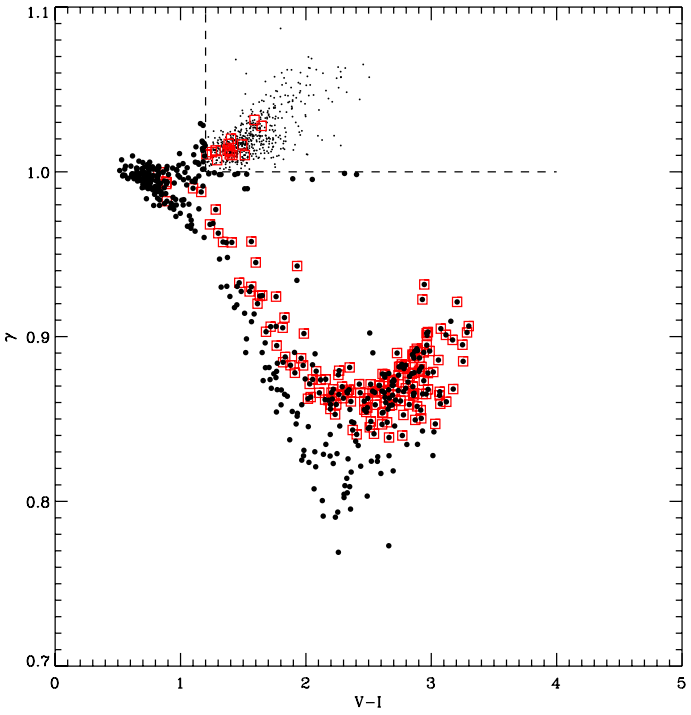

Fig. 8. Gravity index γ as a function of the $V - I$ color (dots). Empty squares are the candidate cluster members selected from their RV and the position on the CMD, and filled circles are objects selected as candidate members from gravity. The dashed line indicates the limit used rejecting giants.

3.6. X-ray detection

X-ray emission is another useful criterion for selecting cluster members in a young cluster. Stellar objects younger than 10^8 yrs, such as those expected to belong to the γ Velorum cluster, are characterized by X-ray fluxes that are significantly larger than those observed in older stars of the same spectral type. In particular, in the 0.5−8.0 keV range, the X-ray luminosity function spans the range between $28 < \log L_X[\mathrm{erg/s}] < 32$, while old solar like stars show values $26 < \log L_X[\mathrm{erg/s}] < 27$ (Favata & Micela 2003; Feigelson et al. 2007). This property allows us to distinguish, in a very efficient way, members in young clusters from field stars that are expected to typically be older and fainter in the X-ray band. The X-ray data can be used here as a membership criterion independent of the spectroscopic methods discussed before.

We used here the X-ray catalog compiled in Jeffries et al. (2009) obtained by using two EPIC-*XMM-Newton* observations performed in 2001. Of the 276 individual sources detected considering the two observations, 260 (255 plus additional five sources with optical counterparts with flagged photometry) have been found in Jeffries et al. (2009) to have an optical counterpart within 6 arcsec, with a very low fraction of expected spurious matches in the PMS region of the CMD where most of the cluster members are expected to be found.

Unfortunately, the *XMM-Newton* observations cover a field of view (FOV) of about 30 arcmin in diameter, where only 307 of the GES targets fall. Of them, only 106 have an X-ray counterpart in the Jeffries et al. (2009) catalog. To these 106 sources we added another four targets (CNAME: J08092860-4720178, J08093332-4718502, J08093364-4722285, J08093920-4721387) not included in the Jeffries et al. (2009) X-ray catalog, despite having a clear X-ray counterpart from visual inspection of the available public EPIC-XMM observations of this field.

In addition, there are five X-ray undetected optical sources (CNAME: J08092576-4730559, J08093321-4722596, J08094171-4726420, J08094519-4719061, and J08103074-4726219) in the Jeffries et al. (2009) catalog that have an ambiguous X-ray identification, because they are close to intense X-ray sources or located in regions with very high background. As in the Jeffries et al. (2009) catalog, we leave these objects as X-ray-undetected and then not consider them as X-ray candidate members.

Figure 9 shows the spatial distribution and the CMD of the 307 targets observed with GES falling in the EPIC-*XMM-Newton* FOV and the 110 X-ray detections. The CMD shows that most of the X-ray detected GES targets follow the cluster region between the 1 and 10 Myr isochrones, while the X-ray undetected targets are outside the cluster region.

4. Final list of members

The membership methods we considered in this work are based on the spectroscopy obtained with the GES data, i.e. the RVs, the Li and Hα lines, and the gravity index, and on photometry from the literature, i.e. the position of candidates in the CMD and the X-ray detections. In this work we do not consider proper motions since available data are limited to bright stars and do not help our analysis. In addition, we note that the S/N limits adopted to define the membership criteria are not the same for all the methods.

As discussed previously, the activity index α_c is derived by measuring the Hα line core, while accretors are defined by measuring the line Hα 10%. This implies that in general the sample of active stars includes the accretors, at least when the α_c index is defined, and thus we did not consider here the accretion as a further membership criterion. We are left with at most six independent criteria.

We considered the gravity index and the photometric criterion as necessary conditions for cluster membership. A further necessary requirement is the dynamical condition based on the RVs, except for stars identified as binaries and fast rotators ($v \sin i > 50\,\mathrm{km\,s^{-1}}$). Indeed, the RVs of these objects can be affected by the presence of double-line series (SB2) or by the lines of one of the two stellar components (SB1). In the case of late type fast rotators, the RVs are strongly affected by the simultaneous presence of molecular bands and broadening of the spectral lines due to the rotation. Thus, even in these cases, the RVs can be affected by very large errors and cannot be used as a necessary condition to select cluster members. The other criteria, EW(Li), activity index from the H_α line, and X-ray emission, are age indicators and are used here to confirm the membership[4].

In summary, to define confirmed members we required that all the following conditions must be fulfilled: (a) they are members based on their gravity and photometry; (b) they are members for RV but this condition is not applied to binaries and/or fast rotators; (c) they are young, meaning that they are members based on their Li or Hα index or X-ray emission. The conditions (a) and (b) include of all possible candidates but have the disadvantage of also including a percentage of contaminants. However with the condition (c) we are confident of cutting the contamination very significantly. The three youth indicators are sensitive in a different way to the spectral types and, in some

[4] This choice automatically excludes any unidentified short-period binaries with RVs outside the cluster RV range.

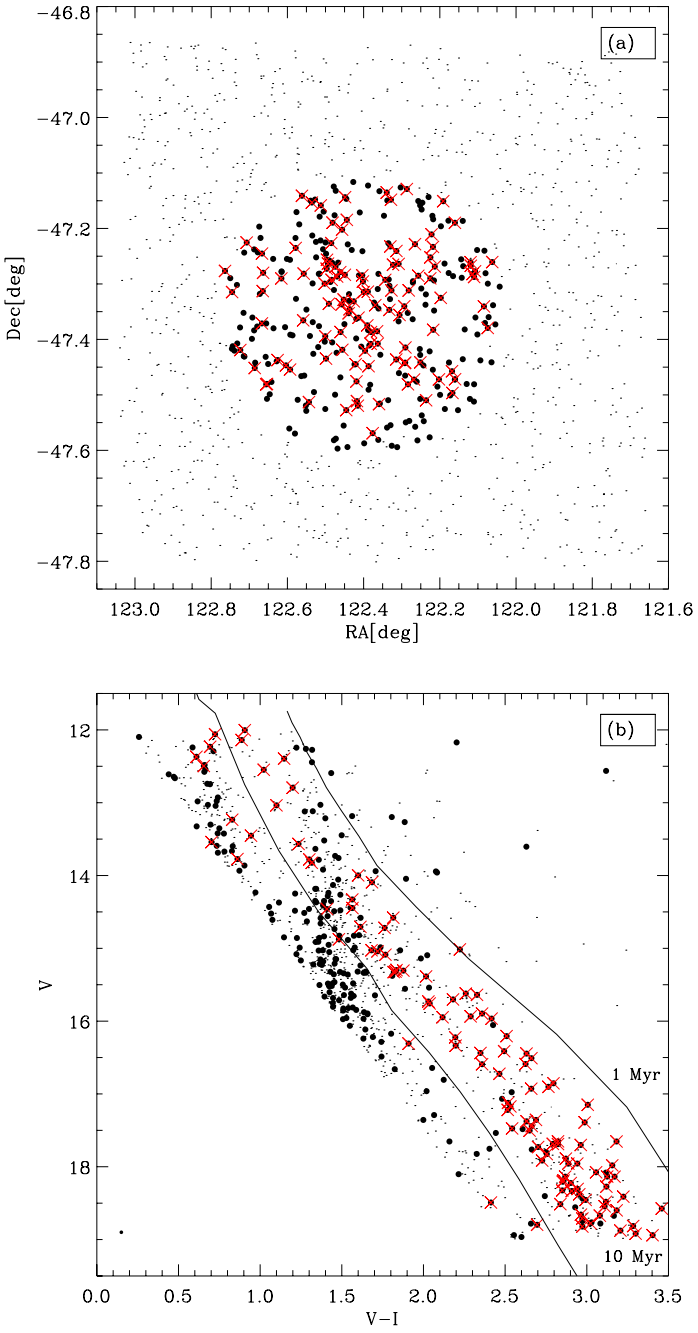

Fig. 9. Spatial distribution (panel **a**)) and CMD (panel **b**)) of all GES targets (dots). Filled large circles are all the targets within the EPIC-*XMM-Newton* FOV, while X symbols are the GES targets with an X-ray counterpart. Solid lines are the 1 and 10 Myr isochrones by Baraffe et al. (2015).

sense, complementary, and then they are used independently to ensure the coverage of the entire spectral type range, especially where the contamination is worst. In fact, the Li indicator is most sensitive to age in the K- and M-type objects (apart from the narrow window in $V - I$ where Li-depleted M dwarfs are found), but is less effective for G-type stars. On the other hand, the rapid spin-down of G-type stars means that X-ray activity is a more effective youth indicator in G- and K-type stars, but less effective for M-type stars with their longer spin-down and activity timescales, (e.g., see discussion in Jeffries 2014).

The three age indicators have a different sensitivity to the stellar ages. In fact, depending on the stellar mass, the lithium depletion starts within a few million years, and then very high EW(Li) values allow us to distinguish very young stars. The X-ray emission and the chromospheric activity are also decreasing as a function of stellar ages but with a longer time scale and are very efficient at selecting low mass stars younger than a few 100 Myr, while the EW(Li) method is more efficient in selecting stars with ages younger than ∼10 Myr. We stress that condition (c) ensures that we also include Li-depleted members with the very unlikey risk of including unidentified field short period binaries at the same cluster distance and with RV consistent with that of the cluster. We note that we have optical photometric membership information for the entire data set of 1242 stars, while the other criteria can be applied only to subsamples. Table 3 shows the number of objects for which each method can be applied and the corresponding number of members selected by that method. In the case of X-ray detections, the number of stars for which we have a membership indication is the total number of optical sources falling in the EPIC-XMM FOV.

Table 3. Number of objects for which we have a membership indication and number of candidate cluster members for each method.

Method	#info	#candidates
G	1043	451
P	1242	579
RV	1221	541
Li	1122	225
A	1176	261
X[a]	307	110

Notes. (G: gravity, P: photometry, RV: radial velocities, Li: lithium, A: chromospheric activity, X: X-ray). [(a)] Only in the EPIC-XMM FOV.

We started the selection by considering only the sample of the 312 candidates for which both the photometry and gravity suggest membership[5]. Among these we considered as confirmed members the 227 objects with RV compatible with the cluster and at least one of the three age indicators consistent with young stars. To these we added 15 stars classified as binaries for which the RV has not been considered but that are members by at least for one of the three age indicators. In total we have 242 confirmed members. This sample includes 28 fast rotators with RV compatible with that of the cluster. In addition, we defined possible members the four fast rotators ($v \sin i > 50$ km s^{-1}) that are members according to Li or H_α or X-rays, but for which the RV is out of the cluster RV range. As already stressed, for these objects the RVs can be unreliable due to the simultaneous presence of molecular bands and line rotational broadening. All the remaining objects are considered non-members. Table 4 summarizes, for the sample of confirmed members, the six criteria used and the number of cases that we find for each combination.

The CMD of the confirmed and possible members is shown in Fig. 10 where the theoretical tracks and isochrones by Baraffe et al. (2015) are also drawn assuming the cluster distance modulus 7.76 mag and $E(V - I) = 0.055$ as in Jeffries et al. (2009). These models were used to derive the stellar masses that are reported in Table 5, together with other fundamental parameters. The 15 binaries classified as cluster members are treated here as single stars. Errors on masses were computed by considering the uncertainties in photometry and the uncertainty in A_V and $E(V - I)$, respectively, for magnitudes and colors, starting from the uncertainty in $E(B - V)$ (0.016), estimated in

[5] For spectra with $S/N < 15$, we considered only the photometric condition, since the gravity index in these cases is poorly defined.

Table 4. Criteria adopted to select confirmed members.

G	P	RV	Li	A	X	M	N	#stars
–	1	0	–	1	0	2	4	1
–	1	1	1	–	–	3	3	11
–	1	1	–	1	–	3	3	4
–	1	1	–	–	1	3	3	1
–	1	1	0	1	–	3	4	2
–	1	1	1	–	0	3	4	1
1	1	1	–	1	–	4	4	17
–	1	1	1	1	–	4	4	19
–	1	1	1	–	1	4	4	6
–	1	1	–	1	1	4	4	6
1	1	1	0	1	–	4	5	4
1	1	1	1	0	–	4	5	1
1	1	1	0	0	1	4	6	1
1	1	1	0	1	0	4	6	1
1	1	1	1	1	–	5	5	79
1	1	1	–	1	1	5	5	6
–	1	1	1	1	1	5	5	17
1	1	1	1	1	0	5	6	6
1	1	1	1	1	1	6	6	57

Notes. Abbreviations for the methods are as in Table 3; (1,0,−) stand for member, non-member, and no information, respectively. M indicates the number of methods for which the membership is positive, while N indicates the number of methods for which the membership information is available. Finally, the number of cases for each combination is given.

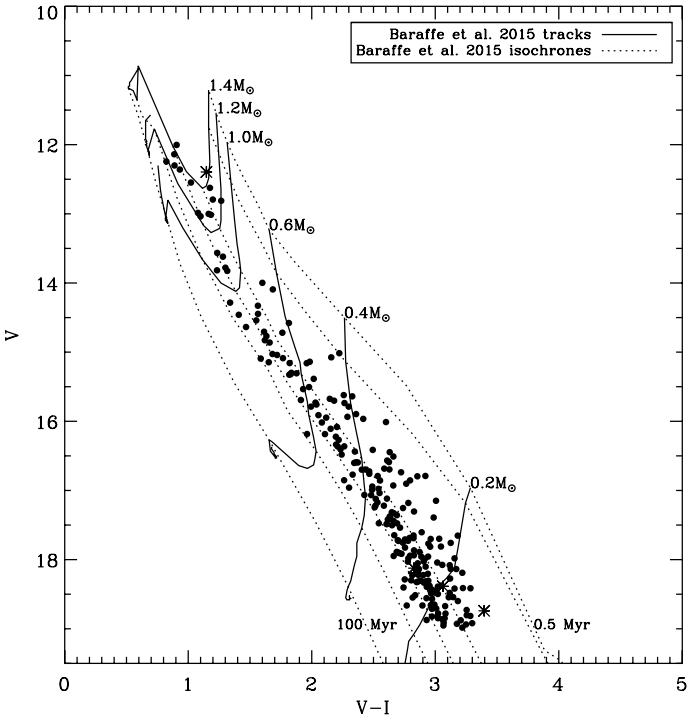

Fig. 10. Color−magnitude diagram of the confirmed (dots) and possible members (crossed dots). Theoretical tracks and isochrones (0.5, 1, 5, 10, 20, and 100 Myr) by Baraffe et al. (2015) are also shown with solid and dotted lines, respectively.

Jeffries et al. (2009). Then, we derived the masses corresponding to the box limits in the CMD defined by these uncertainties.

Since the Baraffe et al. (2015) models are limited to masses lower than 1.4 $M_{\odot}$, we derived a mass value for 237 of the 246 confirmed and possible cluster members. This sample includes objects with masses between 0.16 and 1.3 $M_{\odot}$.

5. Discussion

5.1. Efficiency of the cluster membership methods

As stated in the previous section, to define cluster members we required that the stars have photometric and dynamic (RV) properties consistent with that of the cluster. From this sample we discarded giants by using the gravity index, and this allowed us to significantly reduce the percentage of contaminants.

The three age indicators (EW(Li), α_c and X-rays) have been used to confirm the cluster membership. In most cases the three indicators are consistent, but we have targets for which only one or two criteria give us information on their young age. This can occur for physical reasons, for example if a star already has depleted lithium, or if a star does not show X-ray emission, or for observational reasons, for example if X-ray sensitivity was not sufficient to detect the object. For this reason, to confirm the membership it is sufficient that at least one of the three age indicators is positive.

The results of our membership strategy are given in Table 6 for members within the EPIC-XMM FOV, for which we have six membership criteria and in particular three age indicators. In this table we give the number of confirmed members and the number of objects for which we have a membership indication for each age indicator. The number of confirmed members found with each method with respect to the total sample of confirmed members is also given. Finally, we counted the number of members we would miss if we did not consider that method. The same information is given by splitting the samples into three different color ranges.

The analogous values are given in Table 7 where we consider confirmed members outside of the EPIC-XMM FOV, for which we have five membership criteria and in particular two age indicators. The lowest efficiency of the EW(Li) method for $V-I \lesssim 1$, roughly corresponding to masses >1 $M_{\odot}$, is due to the rapid formation of the radiative core that prevents the Li depletion. Thus in this spectral range, the EW(Li) is not very effective in selecting young stars. In general, these results suggest that all the methods are very effective, since they are positive for at least ~80% of the stars. They are least effective in the regime of M-type stars where some members can be missed. For this reason it is crucial to use, in this spectral range, several age indicators.

The efficiency of the EW(Li) is slightly lower (about 82%) than the other methods for $V-I > 2.4$. The presence of Li is an extremely effective age indicator in M dwarfs since the selected stars are definitively very young, but in the narrow colour range $2.5 < V-I < 3.0$, where Li can be depleted, this method is ineffective in the sense that some members can be missed.

The α_c index, signature of Hα emission, and the X-ray emission, are not very effective at selecting very young stars, since young field stars of spectral type M can also show Hα and/or X-ray emission. But, even if these methods have the disadvantage of including some contaminants, they allow all potential cluster members to be selected. Members can be missed only for observational limitations such as when the S/N of the spectra is <15 and the index cannot be defined, or when they are either objects that are very close to very strong X-ray emitters (M-type stars are typically less bright in X-rays) or faint objects for which the X-ray detection probability is low. Spectra with high S/N and/or X-ray observations with high spatial resolution are required to efficiently use these methods.

We find that within the XMM FOV, the members not retrieved with the Li line are 16 (14 of them are undefined according to Li), while those not identified with the Hα and X-ray methods are 9, over a total of 103 members. The last column of

Table 6. Breakdown of confirmed members in the XMM FOV.

Method	#members	#info	Fraction	Missed
entire $V-I$ range Tot. 103				
Li	87	89	0.84	1
A	94	95	0.91	2
X	94	103	0.91	2
$0.3 < V- < 1.1$ Tot. 4				
Li	2	2	0.50	0
A	4	4	1.00	0
X	4	4	1.00	0
$1.1 < V-I < 2.4$ Tot. 34				
Li	32	33	0.94	0
A	33	34	0.97	0
X	33	34	0.97	1
$2.4 < V-I < 4.1$ Tot. 65				
Li	53	54	0.82	1
A	57	57	0.88	2
X	57	65	0.88	1

Notes. Column 2 is the number of confirmed members found with that method, Col. 3 is the number of confirmed members for which we may apply it, Col. 4 is the ratio with respect to the total number of confirmed members, and Col. 5 is the number of members we would miss if we did not consider that method.

Table 7. Same as Table 6 but for the members in the region outside of the XMM FOV.

Method	#members	#info	Fraction	Missed
Entire $V-I$ range Tot. 139				
Li	110	116	0.79	13
A	126	127	0.91	29
$0.3 < V-I < 1.1$ Tot. 4				
Li	1	1	0.25	0
A	4	4	1.00	3
$1.1 < V-I < 2.4$ Tot. 40				
Li	36	39	0.90	1
A	39	40	0.98	4
$2.4 < V-I < 5.0$ Tot. 95				
Li	73	76	0.77	12
A	83	83	0.87	22

Table 6 gives the total number of members minus the number of members recovered by all other methods but independently of the method indicated in the line. This tells us the number of members that we would miss if we did not use that method. Thus, within the XMM FOV, the three methods are equivalent, and then if we did not use one of them we could still select an almost complete sample of members.

The same is not true if we consider the results in the region outside the XMM FOV where we note that 13 and 29 members would be missed if we did not use the Li or the activity index, respectively. The first group mainly includes the objects with $V-I > 2.7$ that were identified from their very large EW(Li) that would likely be missed by the chromospheric activity method since their spectra have a lower S/N than required, while the latter group includes mainly members with $2.5 < V-I < 3.0$ and $EW(\mathrm{Li}) < 100$ mÅ (18 objects).

We note that this is the region where we estimated finding 20 members and where we did not discard candidate members by leaving the objects undefined according to the Li test (see Sect. 3.3). Thus, these are members of the γ Velorum cluster according to RV, photometry, and gravity, which were confirmed by their chromosperic activity. Even if we do not have confirmation by the Li line that they are very young members, it is very unlikely that they are field stars. In general the number of members detected by X-rays or from activity is not significantly larger than the members found from Li, and this suggests to us that the small differences among the methods are related to their detailed dependence on the spectral range and on the observational strategy.

The number of members found with the three age indicators can be used to pinpoint any age spread among the members. In fact, as discussed in the previous section, the three methods also have different sensitivities to cluster ages. An age spread of a few Myr can only be investigated by using Li, at least for the M dwarfs, while the X-rays and the chromospheric activity are not really age dependent at these ages. Since this cluster is close to the Vela OB2 association, that is expected to be relatively young (<100 Myr), we can, in principle, find more objects selected in X-rays and/or for activity rather than by Li. However, our results suggest that there is no large age spread among members since the number of members selected by using the Li line is comparable to those selected by using the X-ray and the activity methods. Thus we are confident that all selected members originated in the same parent molecular cloud.

5.2. The IMF

According to the GES observational strategy, GIRAFFE targets were selected randomly from a sample of photometric candidates, while the UVES targets were selected within a specific color range in order to discard F-type candidate members that are expected to be fast rotators. This implies that while we are able to estimate the completeness of the sample of confirmed and possible members observed with GIRAFFE, we cannot estimate how complete is the sample of members selected with UVES. For this reason, to derive the IMF of the cluster, we do not consider the targets observed with UVES, and we only use the sample of confirmed and possible members observed with GIRAFFE having masses between 0.16 and 1.3 $M_{\odot}$.

As already mentioned in the Introduction, this cluster includes the two dynamically distinct populations, A and B. However, according to a KS test, we find that the probability that the two populations have statistically indistinguishable mass distributions is 43%. For this reason, we do not consider these two populations separately in the following discussion.

Starting from the sample including the $n_{\mathrm{tot}} = 237$ confirmed and possible members for which we have derived the mass values, the observed IMF has been derived in the linear form,

$$\xi_0(M) = \frac{\mathrm{d}n}{\mathrm{d}M}. \quad (2)$$

The mass bins for the IMF were chosen using the condition $\Delta \log M = 0.15$, which is slightly larger than the typical mass errors. We corrected the IMF for incompleteness by considering for each mass bin the correction factor given by the ratio between the number of all potential photometric candidate members and the number of actually observed targets. These correction factors c for each mass bin and the values of the corrected IMF ($\xi(M) = c\xi_0(M)$) are given in Table 8. The observed and the corrected IMF are shown in Fig. 11. We ignore corrections for photometric completeness because they are small. Jeffries et al. (2009) found that the level of completeness for stars with good photometry fell only slowly from 93% at $V < 16$ to 83% at

Table 8. IMF for the Gamma Vel cluster observed with GIRAFFE.

Mass	ΔN	c	$\xi(M)$
0.16–0.22	54	1.16	4.05 ± 0.55
0.22–0.31	69	1.09	3.45 ± 0.42
0.31–0.44	51	1.11	1.83 ± 0.26
0.44–0.63	28	1.06	0.68 ± 0.13
0.63–0.89	22	1.08	0.39 ± 0.08
0.89–1.25	9	1.12	0.12 ± 0.04

Notes. Column 1 mass bin, Col. 2 number of stars counted in each mass bin, Col. 3 correction factor, and Col. 4 IMF values in the linear form.

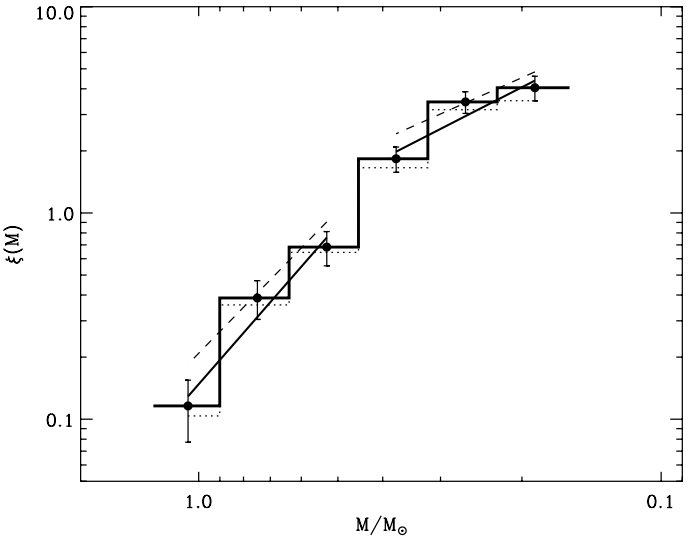

Fig. 11. IMF of the γ Velorum cluster. The dotted line is the IMF derived from the sample of confirmed and possible members of γ Velorum observed with GIRAFFE while the thick solid line is the IMF corrected for incompleteness. The overplotted dashed segments represent the Kroupa (2001) IMF to which we applied an arbitrary vertical shift, while the solid segments show the IMF obtained with our fit.

$19 < V < 20$. We note that for all the considered mass bin, the correction factors are <20%, and this suggests that the observed IMF is not very different from the corrected one.

To derive the IMF parameters we considered the multiple-part power-law IMF of stellar populations, defined by Kroupa (2001) in the form $\xi(M) \propto M^{-\alpha}$. We performed a linear fit of the observed IMF and found $\alpha = 2.6 \pm 0.5$ and $\alpha = 1.1 \pm 0.4$ in the respective mass ranges.

The sample of γ Velorum cluster members used to derive the IMF includes both the resolved SB1 and SB2 binaries that we treated as single stars and an unknown fraction of unresolved binaries. In both cases companions are not included in the star counts. As a result, we compare the observed IMF with the slopes $\alpha = 2.3 \pm 0.5$ for $M > 0.5\ M_\odot$ and $\alpha = 1.0 \pm 0.3$ for $0.15 < M/M_\odot < 0.5$, given by Kroupa et al. (2013) for the primary stars, assuming a binary fraction of 0.5. We note that in Kroupa et al. (2013), the slopes of the primary IMF are equal to those given for the canonical IMF of resolved stellar populations, except in the $0.1 < M/M_\odot < 0.5$, where the canonical stellar IMF slope is $\alpha = 1.3 \pm 0.3$. In Fig. 11 we show the results of the linear fit obtained by us compared to the canonical IMF. This result suggests that the cluster IMF in the low mass range investigated in this work is very similar to the canonical one.

If we consider the mass range used to derive the IMF between 0.16 and 1.3 $M_\odot$, the total mass of the cluster amounts to $\simeq 92\ M_\odot$. By considering the correction for incompleteness, the cluster total mass is $\simeq 100\ M_\odot$. Of course this is a lower limit to the total mass, since it is limited to objects with V fainter than about 12.5 mag. In addition, we did not consider the binary fraction. Nevertheless, even by taking the binary fraction and the star component with mass higher than 1.3 $M_\odot$ into account, the observed cluster total mass is hardly compatible with the presence of γ^2 Vel, whose WC8 component had an initial mass of $\sim 35\ M_\odot$. The expected cluster total mass for a system including a star with mass $\sim 35\ M_\odot$ is $\sim 1000\ M_\odot$ (Weidner et al. 2010), which is significantly higher than the observed one.

Several scenarios have been proposed to explain the formation of γ^2 Vel and the surrounding cluster (Jeffries et al. 2009, 2014; Sacco et al. 2015), and very recently, from N-body modeling, it has been found that population A is in virial equilibrium, while population B is strongly supervirial (Mapelli et al. 2015).

Our analysis does not allow discerning between these scenarios, but the finding that the entire young population, selected in the region around γ^2 Vel, shows a standard IMF suggests that both populations A and B were formed from the same molecular cloud during the same global star formation process.

6. Conclusions

We have analyzed GIRAFFE spectra acquired with the GES project and used several membership indicators. This work allowed us to obtain a list of cluster members whose membership is confirmed by several criteria simultaneously. In addition, thanks to the GES target selection strategy, based on an inclusive sample of candidate members, we were able to obtain a sample of members that is more than 90% complete. These achievements are crucial for studying open clusters, which are usually contaminated by field stars, for which assessing membership is generally very hard.

The GES spectroscopic parameters used as membership indicators are i) radial velocities; ii) equivalent width of the lithium line; iii) α_c index derived by Damiani et al. (2014) from the Hα line that gives indications of chromospheric activity; and iv) gravity γ index defined in Damiani et al. (2014). In addition, we used the optical photometry and the X-ray data of the cluster when available. We obtained a complete list of possible members defined for each method and finally a list of 246 confirmed members that is as reliable and uncontaminated as possible by combining all information.

In particular, radial velocities, photometry, and gravity index were used as necessary conditions to select individual stars, while the youth indicators (i.e., lithium, Hα, and X-ray detections) were used to confirm the membership. For physical reasons or observation limits, youth indicators work best in different spectral regimes. For example, M-type stars with Li are definitely very young, even if the lithium depletion can occur within a few Myr, and then stars with this spectral type can show a wide range of lithium abundance. This implies that by using only the Li criterion, a percentage of cluster members (about 15% in our case) are missed, depending on the cluster age. On the other hand, all the young stars show chromospheric activity or X-ray emission, but depending on their spectral type, they are not necessarily very young. Nevertheless, if used in combination with other conditions, such as RV, gravity, and photometry, the activity and X-ray criteria are very useful in selecting cluster members and allow us to also recover those missed according to the Li line in the M-type spectral range. Since our selection starts from a sample of candidate members for RV, photometry,

and gravity, the three youth indicators were used indifferently to confirm the membership.

Finally, by using the new theoretical models by Baraffe et al. (2015), we derived the masses for 237 of the 246 confirmed and possible members that are in the range [0.16,1.3] $M_{\odot}$. We derived the cluster IMF by taking the incompleteness due to the unobserved members into account. We compared the derived IMF with the multiple-part power-law IMF form given in Kroupa (2001) and found that the IMF slope is $\alpha = 2.6 \pm 0.5$ for $0.5 < M/M_{\odot} < 1.3$ and $\alpha = 1.1 \pm 0.4$ for $0.16 < M/M_{\odot} < 0.5$. These values are consistent with a canonical IMF.

Finally, we found that the total mass of the cluster component with $0.16 < M/M_{\odot} < 1.3$ is about $100\,M_{\odot}$ which is significantly lower than expected for a cluster in which a star of $\sim 35\,M_{\odot}$ formed. The observed IMF suggests us that the two kinematically distinct populations A and B found by Jeffries et al. (2014) were formed from the same molecular cloud in the same global star formation process.

Acknowledgements. This research made use of data products from observations made with ESO Telescopes at the La Silla Paranal Observatory under Program ID 188.B-3002. These data products have been processed by the Cambridge Astronomy Survey Unit (CASU) at the Institute of Astronomy, University of Cambridge, and by the FLAMES/UVES reduction team at INAF/Osservatorio Astrofisico di Arcetri. These data were obtained from the *Gaia*-ESO Survey Data Archive, prepared and hosted by the Wide Field Astronomy Unit, Institute for Astronomy, University of Edinburgh, which is funded by the UK Science and Technology Facilities Council. This work was partly supported by the European Union FP7 program through ERC grant number 320360 and by the Leverhulme Trust through grant RPG-2012-541. We acknowledge the support from INAF and Ministero dell' Istruzione, dell' Università' e della Ricerca (MIUR) in the form of the grant "Premiale VLT 2012". The results presented here benefit from discussions held during the *Gaia*-ESO workshops and conferences supported by the ESF (European Science Foundation) through the GREAT Research Network Program.

References

Baraffe, I., Homeier, D., Allard, F., & Chabrier, G. 2015, A&A, 577, A42
Bertout, C., Harder, S., Malbet, F., Mennessier, C., & Regev, O. 1996, AJ, 112, 2159
Bochanski, J. J., Munn, J. A., Hawley, S. L., et al. 2007, AJ, 134, 2418
Damiani, F., Prisinzano, L., Micela, G., et al. 2014, A&A, 566, A50
De Marco, O., & Schmutz, W. 1999, A&A, 345, 163
de Zeeuw, T. 1999, in The Third Stromlo Symposium: The Galactic Halo, eds. B. K. Gibson, R. S. Axelrod, & M. E. Putman, ASP Conf. Ser., 165, 515
Eldridge, J. J. 2009, MNRAS, 400, L20
Favata, F., & Micela, G. 2003, Space Sci. Rev., 108, 577
Feigelson, E., Townsley, L., Güdel, M., & Stassun, K. 2007, in Protostars and Planets V, eds. B. Reipurth, D. Jewitt, & K. Keil, 313
Frasca, A., & Catalano, S. 1994, A&A, 284, 883
Frasca, A., Biazzo, K., Lanzafame, A. C., et al. 2015, A&A, 575, A4
Gilmore, G., Randich, S., Asplund, M., et al. 2012, The Messenger, 147, 25
Hernández, J., Hartmann, L., Calvet, N., et al. 2008, ApJ, 686, 1195
Jackson, R. J., Jeffries, R. D., Lewis, J., et al. 2015, A&A, 580, A75
Jeffries, R. D. 2014, in EAS Pub. Ser., 65, 289
Jeffries, R. D., Naylor, T., Walter, F. M., Pozzo, M. P., & Devey, C. R. 2009, MNRAS, 393, 538
Jeffries, R. D., Jackson, R. J., Cottaar, M., et al. 2014, A&A, 563, A94
Kroupa, P. 2001, MNRAS, 322, 231
Kroupa, P., Weidner, C., Pflamm-Altenburg, J., et al. 2013, The Stellar and Sub-Stellar Initial Mass Function of Simple and Composite Populations, 115
Lanzafame, A. C., Frasca, A., Damiani, F., et al. 2015, A&A, 576, A80
Mapelli, M., Vallenari, A., Jeffries, R. D., et al. 2015, A&A, 578, A35
Muzerolle, J., Briceño, C., Calvet, N., et al. 2000, ApJ, 545, L141
Pasquini, L., Avila, G., Blecha, A., et al. 2002, The Messenger, 110, 1
Pozzo, M., Jeffries, R. D., Naylor, T., et al. 2000, MNRAS, 313, L23
Sacco, G. G., Jeffries, R. D., Randich, S., et al. 2015, A&A, 574, L7
Sestito, P., Randich, S., Mermilliod, J.-C., & Pallavicini, R. 2003, A&A, 407, 289
Siess, L., Dufour, E., & Forestini, M. 2000, A&A, 358, 593
Spina, L., Randich, S., Palla, F., et al. 2014, A&A, 567, A55
Traven, G., Zwitter, T., Van Eck, S., et al. 2015, A&A, 581, A52
Weidner, C., Kroupa, P., & Bonnell, I. A. D. 2010, MNRAS, 401, 275
White, R. J., & Basri, G. 2003, ApJ, 582, 1109